

Domain wall induced spin-polarized flat bands in antiferromagnetic topological insulators

E. K. Petrov,^{1,2,*} V. N. Men'shov,^{3,1,2} I. P. Rusinov,^{1,2} M. Hoffmann,⁴ A. Ernst,^{4,5}
M. M. Otrokov,^{6,7} V. K. Dugaev,⁸ T. V. Menshchikova,¹ and E. V. Chulkov^{9,10,2,6,1,†}

¹*Tomsk State University, 634050 Tomsk, Russia*

²*St. Petersburg State University, 199034 St. Petersburg, Russia*

³*NRC Kurchatov Institute, 123182 Moscow, Russia*

⁴*Institute for Theoretical Physics, Johannes Kepler University, 4040 Linz, Austria*

⁵*Max Planck Institute of Microstructure Physics, 06120 Halle, Germany*

⁶*Centro de Física de Materiales (CFM-MPC), Centro Mixto CSIC-UPV/EHU,
20018 Donostia-San Sebastián, Basque Country, Spain*

⁷*IKERBASQUE, Basque Foundation for Science, 48011 Bilbao, Spain*

⁸*Department of Physics and Medical Engineering,
Rzeszów University of Technology, 35-959 Rzeszów, Poland*

⁹*Departamento de Física de Materiales, Facultad de Ciencias Químicas,
Universidad del País Vasco, Apdo. 1072, 20080 San Sebastián/Donostia, Spain*

¹⁰*Donostia International Physics Center (DIPC), 20018 San Sebastián/Donostia, Spain*

(Dated: February 1, 2022)

A flat band in fermionic system is a dispersionless single-particle state with a diverging effective mass and nearly zero group velocity. These flat bands are expected to support exotic properties in the ground state, which might be important for a wide range of promising physical phenomena. For many applications it is highly desirable to have such states in Dirac materials, but so far they have been reported only in non-magnetic Dirac systems. In this work we propose a realization of topologically protected spin-polarized flat bands generated by domain walls in planar magnetic topological insulators. Using first-principles material design we suggest a family of intrinsic antiferromagnetic topological insulators with an in-plane sublattice magnetization and a high Néel temperature. Such systems can host domain walls in a natural manner. For these materials, we demonstrate the existence of spin-polarized flat bands in the vicinity of the Fermi level and discuss their properties and potential applications.

PACS numbers: 71.20.-b, 73.20.At, 75.25.-j

I. INTRODUCTION

The modern technology proposals require the consideration of quantum effects, which will significantly expand the functionality of new spintronic devices. Of great importance is realization of such physical phenomena as various Hall effects¹⁻³, a gate-tunable topological valley transport⁴⁻⁸ and superconductivity⁹⁻¹³. In many cases, it can be attained using specific electron states – flat bands – which can arise either because of strong electronic correlations¹⁴⁻¹⁷ or due to specific structural deformations^{18,19}. In absence of strongly correlated electrons, flat bands can be induced by strain and were previously found in a number of non-magnetic materials such as IV-VI semiconductor multilayers including topological crystalline insulators^{18,20,21}, and, recently, in twisted bilayer graphene^{19,22}. In magnetic topological materials such states have never been reported so far.

We propose a way to generate flat bands in magnetic topological insulators (TIs) surfaces, where massless Dirac states and the exchange fields can serve as a platform to create spin-polarized dispersionless states. The latter can appear due to magnetic domain walls (DWs) at the surface. However, most magnetic TIs are not well appropriated for such a realization of flat bands,

either because of a relatively low critical temperature (Curie or Néel temperature) or because of strong disorder effects in magnetically doped TIs. In this context, a universal platform can be provided by van der Waals (vdW) layered antiferromagnetic topological insulators (AFM TIs)²³⁻³⁰, where topological phase is governed by the $S = \Theta T_{1/2}$ symmetry, with Θ and $T_{1/2}$ being time-reversal and primitive-lattice translation operators, respectively³¹.

As any other magnets, magnetic vdW compounds may manifest a domain structure³², which ensures the existence of antiphase domain walls. Just recently Sass and coauthors have reported on the visualization and manipulation of DWs in the out-of-plane AFM TI $\text{MnBi}_{2-x}\text{Sb}_x\text{Te}_4$ ³³. When such a DW appears in the AFM TI bulk, it can be terminated at the sample surface. Magnetic DWs on AFM TI surface could also be induced intentionally using the tip of a magnetic force microscope³⁴ or by spatially modulated external magnetic field due to Meissner repulsion from a bulk superconductor³⁵, as it has been realized in Cr-doped TI $(\text{Bi,Sb})_2\text{Te}_3$. Note also that a structural step can cause the formation of antiphase DW at rough surface of vdW AFM material in which sublattice magnetization direction alternates along the stacking direction.

Here, using our experience in first-principles design

of topological insulators^{27,36,37}, we suggest a number of AFM TI candidates with in-plane sublattice magnetization (planar AFM TIs in the following text) in the family of vdW systems MPn_2Ch_4 ($M=Mn, V$; $Pn=Bi, Sb$; $Ch=Se, Te$). Remarkably, the proposed V-based compounds have a significantly higher Néel temperature (in the range of 77 – 94 K) than Mn-based AFM TIs and related systems^{37–41}. We verify the shift of the gapless Dirac cone in momentum space in the compounds under study. Employing a tight-binding and a model Hamiltonian approaches, we demonstrate that antiphase DW induces a bound surface state with peculiar characteristics: it is topologically protected, dispersionless (flat) and exhibits out-of-plane spin polarization. Also we show that by applying an external magnetic field perpendicular to the surface it is possible to tune the characteristics of this DW induced state. In view of the unique combination of two distinctive properties, flat bands and planar magnetic TIs, we suggest several potential applications such as optical spin manipulations, anomalous Hall effect and superconductive coupling between the neighboring DWs.

II. RESULTS AND DISCUSSION

Based on total energy arguments we theoretically verified that the V-based materials (VBi_2Se_4 , $VBi_2Te_2Se_2$, VBi_2Te_4 , $VSb_2Te_2Se_2$, VSb_2Te_4) and $MnBi_2Te_2Se_2$ (see Table I) energetically stable (see Supplementary Table 1). As the related compounds tend to crystallize either in monoclinic ($C2/m$ space group) or rhombohedral ($R\bar{3}m$ space group, Fig. 1a) structure⁴², we compared total energies in these two phases for each compound and found that the latter phase is Preferable (see Supplementary Table 2). It is important to note, that the crystal structure in this phase can be represented by hexagonal septuple layer (SL) blocks (e.g., Te - Bi - Se - V - Se - Bi - Te in the case of $VBi_2Te_2Se_2$), separated by vdW gaps. For more details of calculations see Supplementary Note 1 and Supplementary Table 3.

Since the interlayer magnetic coupling in similar vdW systems was found to be rather weak compared to the intralayer one^{32,37,38}, we consider first the magnetic order in a single SL. Total energy calculations show ferromagnetic configuration to be preferable of the three considered magnetic configurations, ferromagnetic (FM), collinear antiferromagnetic (cAFM) and non-collinear antiferromagnetic (ncAFM). Taking into account the interlayer magnetic coupling, total energy calculations reveal the antiparallel alignment of magnetic moments in adjacent SLs in the bulk materials (see Table I). These results are supported by the calculated exchange coupling parameters (Fig. 1b), which are mostly positive for the intralayer interaction ($J_{||}^{0,i}$) indicating FM order, whereas the interlayer exchange parameters $J_{\perp}^{0,i}$ are mostly negative, which is a distinct feature of the interlayer AFM order.

To calculate the magnetocrystalline anisotropy energy

(MAE), we consider three different spin quantization axis orientations: [0001] (out-of-plane), [1010] and [1100] (in-plane). All considered compounds were found to tend to in-plane magnetization (see Table I). $MnBi_2Te_2Se_2$ is the only compound which stands out, because its in-plane magnetization is due to a strong dipole-dipole contribution to MAE. We did not find any significant in-plane MAE.

We note the remarkable difference between the V- and Mn-containing compounds. The vdW systems under consideration possess a layered structure, where FM layers are well separated, and the interlayer exchange coupling J_{\perp} is much weaker than the intralayer one $J_{||}$. Typically, in layered systems, the magnetocrystalline anisotropy and the interlayer exchange coupling are essential for establishing a magnetic order at finite temperature. If a two-dimensional magnet has a continuous symmetry in spin space, there is no spontaneous magnetization at finite temperatures^{43,44}. For the proposed planar AFM TIs, within the framework of our calculation accuracy, we have not been able to identify a preferable orientation of Mn (or V) sublattice magnetization relative to crystallographic axes in the basal plane. It means that these planar AFM TIs are highly sensitive to orientational thermal fluctuations, which are expected to hinder the establishment of an intrinsic long-range magnetic order. This is in contrast to AFM TI $MnBi_2Te_4$, which is an Ising magnet with out-of-plane easy axis.

Our calculations show that the interlayer exchange coupling in the V-containing compounds is one or two orders of magnitude larger than in $MnBi_2Te_2Se_2$ and $MnBi_2Te_4$ ³⁷ (see Fig. 1b). The underlying cause is as follows. As follows from the density of states (DOS) plots, Mn $3d$ -states are located far away from the Fermi level at $\simeq -6$ eV and overlap only marginally with p -bands of Bi, Te and/or Se, implying the main effect of Mn to introduce the exchange field into SL block (see Fig. 1e). In contrast, $3d$ -states of vanadium hybridize significantly the p -states of Bi/Te/Se within a wide energy range, which provides a very strong superexchange coupling between neighboring SLs across the vdW gap. As a result, vanadium compounds exhibit Néel temperature T_N above 75 K, which is about nearly 4 times higher than in the case of $MnBi_2Te_2Se_2$ (see Table I). It should be noted that predicted $MnBi_2Te_2Se_2$ T_N is slightly lower than in the case of out-of-plane magnetized AFM TI $MnBi_2Te_4$ (24.3 K)³⁷. The Néel temperature can be roughly estimated within the standard spin-wave theory, $T_N^{SW} \sim \frac{J_{||}S^2}{\ln(\vartheta \frac{J_{||}}{J_{\perp}})}$ (ϑ is a model parameter of the order of π^2). Then it is clear that an increase of the interlayer coupling by one or two orders of magnitude leads to three- or fourfold growth of the Néel temperature, which is in qualitative agreement with the calculation results presented in Table I. Thus, the enhanced interlayer interaction due to hybridization of the p -states of Bi/Te/Se and the $3d$ -states of V is crucial to stabilize a long-range AFM order at such high temperatures.

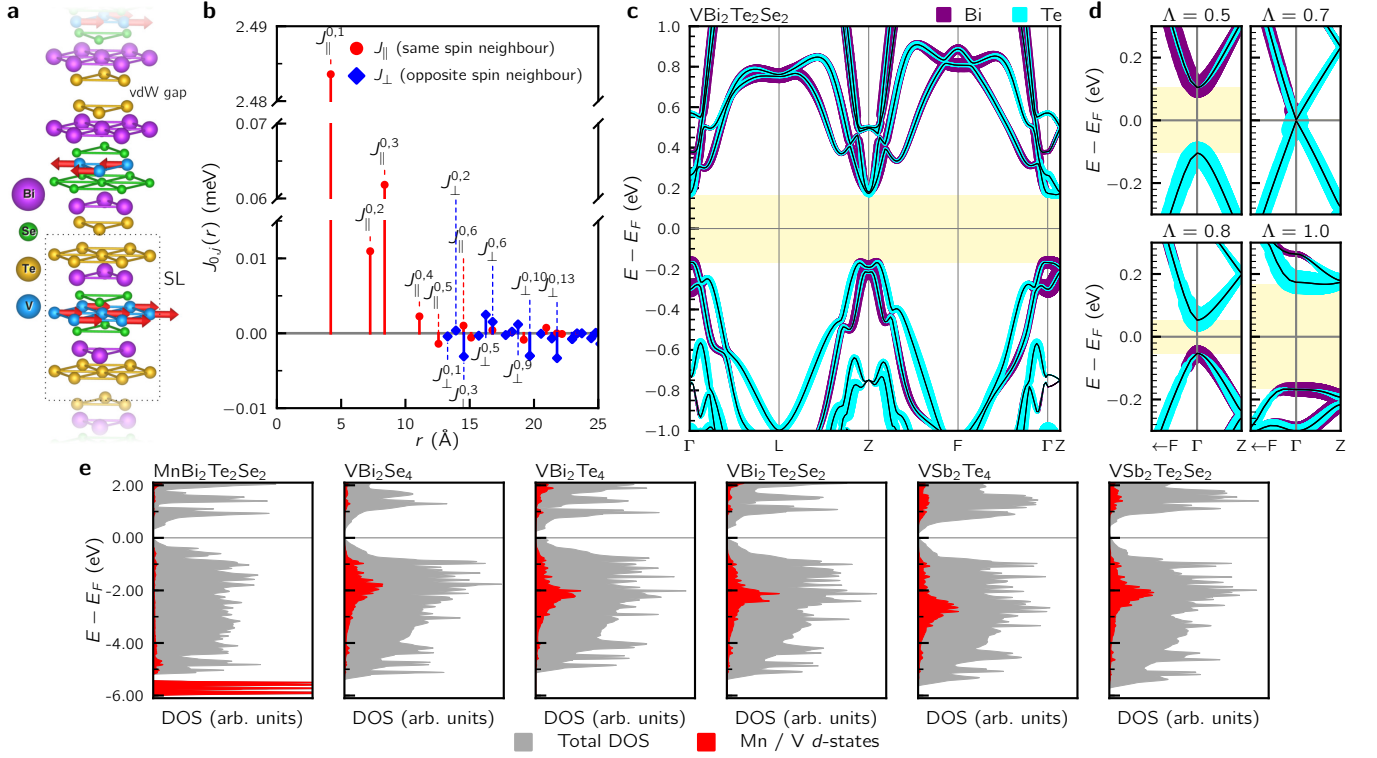


FIG. 1. (a) Crystal structure of bulk $\text{VBi}_2\text{Te}_2\text{Se}_2$. (b) Calculated exchange parameters $J^{0,j}$ for the intralayer (J_{\parallel} , red circles) and interlayer (J_{\perp} , blue diamonds) pair interactions as a function of the V–V distance $r_{0,j}$ for $\text{VBi}_2\text{Te}_2\text{Se}_2$. (c) $\text{VBi}_2\text{Te}_2\text{Se}_2$ bulk band structure. The energies are given with respect to the Fermi level E_F . The band gap is highlighted with light yellow. The orbital composition is represented by colored lines, whose thickness is proportional to a specific site contribution to the electron state. (d) Bulk $\text{VBi}_2\text{Te}_2\text{Se}_2$ band structure in the vicinity of Γ point at different values of the SOC constant Λ (SOC is not taken into account with $\Lambda = 0$, and fully taken into account with $\Lambda = 1$). The orbital composition is also present. (e) Bulk DOS of considered compounds (total and projected on Mn or V sites). Note, here the Fermi level is positioned at valence band top.

TABLE I. Differences in total energies between FM (E_{FM}^{intra}), cAFM (E_{cAFM}^{intra}) and nCAFm (E_{ncAFM}^{intra}) SL slab magnetic configurations and FM (E_{FM}^{inter}) and AFM (E_{AFM}^{inter}) bulk magnetic orders. Differences in total energies of in plane (E_{\parallel}) and out of plane (E_{\perp}) spin quantization axis orientations, also including the dipole-dipole contribution (E_{dip}). Magnetic moments on Mn or V sites. Calculated Néel temperatures T_N . Bulk band gap. Z_2 invariant value.

Compound	$\text{MnBi}_2\text{Te}_2\text{Se}_2$	VBi_2Se_4	$\text{VBi}_2\text{Te}_2\text{Se}_2$	VBi_2Te_4	$\text{VSb}_2\text{Te}_2\text{Se}_2$	VSb_2Te_4
$E_{cAFM}^{intra} - E_{FM}^{intra}$ (meV/f.u.)	+5.1	+9.2	+13.9	+16.6	+11.6	+12.3
$E_{ncAFM}^{intra} - E_{FM}^{intra}$ (meV/f.u.)	+6.8	+17.6	+25.7	+29.9	+14.9	+15.5
$E_{AFM}^{inter} - E_{FM}^{inter}$ (meV/f.u.)	-0.770	-0.164	-0.320	-0.677	-0.387	-0.788
$E_{\parallel} - E_{\perp}$ (meV/f.u.)	+0.053	-0.092	-0.311	-0.176	-0.004	-0.087
$E_{\parallel} - E_{\perp} + E_{\parallel}^{dip}$ (meV/f.u.)	-0.078	-0.148	-0.363	-0.224	-0.059	-0.138
Magnetic moment (μ_B)	4.622	2.924	2.933	2.956	2.936	2.966
T_N (K)	18.6	80.88	77.1	78.6	91.6	93.9
Band gap (meV)	256	55	334	233	11	125
Z_2	1	0	1	1	0	1

In order to be sure that the resulting magnetic structures are stable against relatively small lattice parameter perturbations, which may be induced during growth process, we studied the dependence of the magnetic structure on lattice constant values which were varied within $\pm 3\%$ from the equilibrium value. Resulting equilibrium magnetic structures were found to be insensitive to such

perturbations.

All considered compounds have typical narrow-gap semiconductor band structures with a band gap ranging from 11 meV up to 334 meV (see Fig. 1c and Table I, also see Supplementary Note 2 and Supplementary Figure 2). We found that the $\text{MnBi}_2\text{Te}_2\text{Se}_2$, $\text{VBi}_2\text{Te}_2\text{Se}_2$, VBi_2Te_4 and VSb_2Te_4 band gaps are inverted, which is confirmed

by \mathbb{Z}_2 invariant calculations, which show $\mathbb{Z}_2 = 1$. In contrast, VBi_2Se_4 and $\text{VSb}_2\text{Te}_2\text{Se}_2$ were found to have a trivial insulating bulk band structure with $\mathbb{Z}_2 = 0$. In order to track the band gap inversion genesis, we calculated $\text{VBi}_2\text{Te}_2\text{Se}_2$ bulk band structure at different spin-orbit coupling (SOC) weighted with a parameter Λ ranging from 0 (SOC not accounted) to 1 (SOC fully accounted). The results clearly show that orbital composition of the band gap edges at $\Lambda < 0.7$ is not inverted yet: highest valence band is primarily formed by Te states, and lowest conduction band by Bi states. At $\Lambda \approx 0.7$ the band gap vanishes and at $\Lambda > 0.7$ it reopens with inverted edges (see Fig. 1d). The inversion is caused mainly by p_z states of ions close to vdW gaps (Te and Bi), similar to tetradymite-like non-magnetic TIs. Other topologically nontrivial compounds under study exhibit a similar behavior.

The inversion ensures the appearance of a topological surface state (TSS) on the (0001) surface of $\text{MnBi}_2\text{Te}_2\text{Se}_2$, $\text{VBi}_2\text{Te}_2\text{Se}_2$, VBi_2Te_4 and VSb_2Te_4 . As an example, Fig. 2a presents the spectrum of such surface state of $\text{VBi}_2\text{Te}_2\text{Se}_2$. As may be seen from the inset, the Dirac point is slightly shifted from the $\bar{\Gamma}$. The direction of the shift is normal to the magnetization \mathbf{M} of the topmost SL, and its value is proportional to its magnitude $|\mathbf{M}|$. Surface band structures of the other topologically non-trivial compounds can be found in Supplementary Note 2 and Supplementary Figure 3. Thus, our DFT calculations demonstrate that all the topologically nontrivial compounds under study are characterized by a gapless Dirac state with a helical spin texture on the ideal (0001) surface.

The right panel in Fig. 2a indicates that the Dirac fermions are predominantly localized within the topmost SL. Their behavior, affected by the exchange field, $\sim \mathbf{M}$, originated from the local moments of the same SL, can be described by an effective two-dimensional Hamiltonian

$$H(\mathbf{k}) = v(k_y\sigma_x - k_x\sigma_y) - j(M_x\sigma_x + M_y\sigma_y) - j_\perp\sigma_zM_z, \quad (1)$$

where v is the Fermi velocity, $\mathbf{k} = (k_x, k_y)$ is the in-plane momentum, σ_x , σ_y and σ_z are the Pauli matrices acting in spin space. For the definiteness, we assign $j, j_\perp > 0$ and $v > 0$. The first term captures the presence of the Dirac-like quasiparticles with a linear spectrum and a perfect spin-momentum locking. The effective exchange integrals j and j_\perp couple the surface quasiparticle spins with the local magnetization of the uppermost SL, $\mathbf{M} = (M_x, M_y, M_z)$, which can generically be in an arbitrary direction. In the case of the spatially homogeneous magnetization \mathbf{M} , the energy spectrum of the Hamiltonian (1) is given by the relation $E^2(\mathbf{k}) = (vk_x + jM_y)^2 + (vk_y - jM_x)^2 + j_\perp^2 M_z^2$.

To explore how the spatially inhomogeneous magnetization $\mathbf{M}(x, y)$ affects the surface state of AFM TI, we use a model of a single rigid DW. In Hamiltonian (1) the (x, y) plane is assumed to be divided in two semi-infinite uniformly ordered regions with opposite polarizations so that $\mathbf{M}(x, y)$ changes its direction upon cross-

ing the linear boundary $x = 0$, but keeps its magnitude. We specify the space profile of the DW in the form $\mathbf{M}(x, y) = M_0(\sin\theta h(x), 0, \cos\theta)$, where $h(x)$ is the Heaviside function, $|\mathbf{M}(x, y)| = M_0 = \text{const}$. Here the magnetization vector can rotate through an angle $\pi - \theta$ out of the plane. Due to the periodicity along \mathbf{y} direction, the momentum k_y is a good quantum number. To describe the fermion state hosted by the DW we apply the analytical approach as well as the numerical tight-binding calculations.

In following, we address the planar AFM TI surface where the local moments lie in the plane and have opposite directions in the right and left domains, i.e. $\mathbf{M}(x, y) = M_0(h(x), 0, 0)$ (see Fig. 2b). The surface with such "tail-to-tail" DW harbors two types of quasiparticles manifesting utterly distinct behaviors: on the one hand, the 2D *massless* Dirac fermions; on the other hand, the 1D heavy fermions with *infinitely large effective mass*. The pair of the Dirac cones, shifted to momenta $\pm k_0$, where $k_0 = \frac{jM_0}{v}$, with respect to the Brillouin zone center, corresponds to the two semi-infinite domains with opposite magnetization. The flat band exists within the interval between the Dirac nodes, $|k_y| < k_0$. Remarkably, this particular state does not disperse in k_y at zero energy, $E(\mathbf{k}) = 0$, forming a sharp peak in DOS at $E = 0$ against the linear dependence of Dirac fermions DOS (see right panel on Fig. 2b). This flat band state is topologically protected, which is originated from the Berry phase of π for each Dirac node, and, therefore, can not be destroyed by DW imperfections. The probability density of the flat band decays exponentially away from the DW on the scale $|\chi(x)|^2 \sim \exp(-2k_0|x|)$ as demonstrated in Fig. 2c. Furthermore, the dispersionless state is fully spin polarized. Therefore, the expectation value of the spin angular momentum is zero for the in-plane components, $\langle\sigma_x\rangle = \langle\sigma_y\rangle = 0$, but it is non-zero in the direction normal to the surface, i.e., normal to the easy plane, $\langle\sigma_z\rangle \neq 0$. Note, the spin polarization of the flat band induced by the "head-to-head" DW is antiparallel to the one induced by the "tail-to-tail" DW.

In general, the surface magnetization can not be attached tightly to the plane. For example, Mn or V sublattice magnetization of a planar AFM TI can acquire non-zero out-of-plane component M_z due to an external magnetic field or magnetic proximity effect. In the case of an AFM TI surface hosting an isolated DW with the spatial profile $\mathbf{M}(x, y) = M_0(\sin\theta h(x), 0, \cos\theta)$, the uniform out-of-plane component M_z breaks the spin degeneracy opening the energy gaps at the Dirac points $\pm k_0 \sin\theta$ in the spectrum (see Fig. 3b,c). As follows from the figures, "tail-to-tail" DW creates the dispersionless state with the energy $E = j_\perp M_z$ ($E = -j_\perp M_z$), which connects the band edges of the two gapped cones with dispersion $E^2(\mathbf{k}) = (vk_x)^2 + v^2(k_y \pm k_0 \sin\theta)^2 + j_\perp^2 M_z^2$. Correspondingly, the keen peak in the density of states appears just at the band edge. Indeed we observe such a gap opening within *ab-initio* calculations when the perfect planar AFM phase is subjected to an out-of-plane

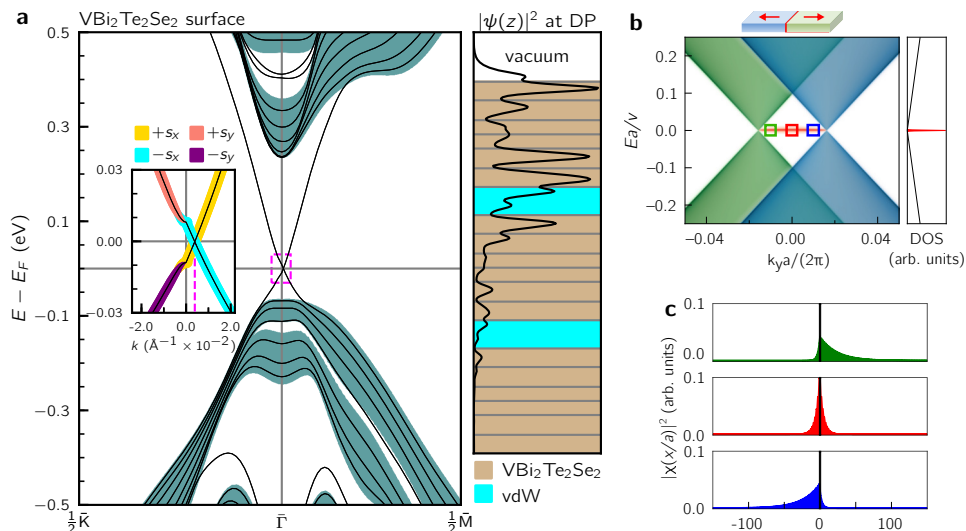


FIG. 2. **(a)** $\text{VBi}_2\text{Te}_2\text{Se}_2$ surface band structure near the Fermi level. Sea-blue areas lines correspond to bulk bands, projected on two-dimensional Brillouin zone (2D BZ), and the black lines to surface bands. Surface spin texture (inset on the left) is represented by color lines, which thickness is proportional to spin projection value. The right panel depicts $|\psi(z)|^2$ at Dirac point (DP), with ψ being one-electron wavefunction. **(b)** Spectral density of the electron states on the surface containing single antiphase DW. For generality, the scales of the axes are presented in dimensionless units constructed by combination of energy and momentum with model parameters. The spectral density corresponding to the left (right) semi-infinite region is represented by blue (green) color, and flat band by red color. DOS at the $\bar{\Gamma}$ point of 2D BZ is shown on the right side of the panel. Black solid line represents DOS for the Dirac cones, the red peak is DOS for the flat band. The magnetic configuration is schematically illustrated on the top so that red arrows in blue and green regions indicate magnetization directions in the vicinity of DW. **(c)** The charge density distribution of zero-energy bound states as a function of distance from the DW. The energy-momenta values are marked by color squares in the panel **(b)**.

Zeeman perturbation. The latter contributes to the gap opening at the Dirac point in the surface state spectrum of $\text{MnBi}_2\text{Te}_2\text{Se}_2$ (see Fig. 3a).

According to the numerical simulations, $\text{MnBi}_2\text{Te}_2\text{Se}_2$ is vdW AFM TI with in-plane anisotropy, whereas MnBi_2Te_4 has been identified as an out-of-plane AFM TI. Therefore, it is natural to assume that the solid solution $\text{MnBi}_2(\text{Te}_{1-x}\text{Se}_x)_4$ at the certain value $0 < x < \frac{1}{2}$ would have an AFM order with the sublattice magnetization directed to the angle $0 < |\theta| < \frac{\pi}{2}$ to the basal plane, keeping nontrivial invariant $\mathbb{Z}_2 \neq 0$. In our approach, in the presence of the antiphase DW, the surface magnetization of such a material is modelled with the spatial profile $\mathbf{M}(x, y) = M_0(\sin \theta h(x), 0, \cos \theta h(x))$. Interestingly, the DW induced bound state is associated with the linear spectral branch, $E(k) = \pm \frac{j_{\perp}}{j} \cot \theta v k_y$, which spans the magnetic gap, $2|j_{\perp} M_0 \cos \theta|$, and connects edges of the bands originated from the opposite magnetic domains (see Fig. 3d, e). Thus, the surface band structure of vdW AFM TI materials can be tuned by different factors (such as chemical composition, strain, etc.) to change the properties of the DW bound state from almost a dispersionless band (with huge mass) to a massless band near the Fermi level.

III. CONCLUSION

In this paper we proposed a tetradymite-like planar AFM TI family and by means of *ab initio* calculations we determined their equilibrium crystal, electronic and magnetic structure. We found all considered compounds to be layered antiferromagnets with an in-plane magnetization.

The proposed V-based compounds have Néel temperature in the range of 77 – 94 K, which is significantly higher than in the case of Mn-based AFM TIs. We showed that the critical temperature can strongly depend on the chemical composition, in particular, Sb-containing compounds show increasing Néel temperature of almost 20 K with respect to Bi ones. All the considered compounds possess a typical semiconductor bulk band structure. We found bulk $\text{MnBi}_2\text{Te}_2\text{Se}_2$, $\text{VBi}_2\text{Te}_2\text{Se}_2$, VBi_2Te_4 and VSb_2Te_4 to exhibit $\mathbb{Z}_2 = 1$ and an AFM TI phase. Such compounds are characterized by a gapless surface state on the (0001) surface, which has a helical spin texture similar to a nonmagnetic TI. The topmost SL magnetization shifts Dirac point from $\bar{\Gamma}$.

We demonstrated that magnetic inhomogeneities likes DWs on the (0001) surface can prompt the appearance of topological one-dimensional flat bands, which give rise to a sharp peak in the DOS near the Fermi level. We showed that flat band states can be effectively tuned by

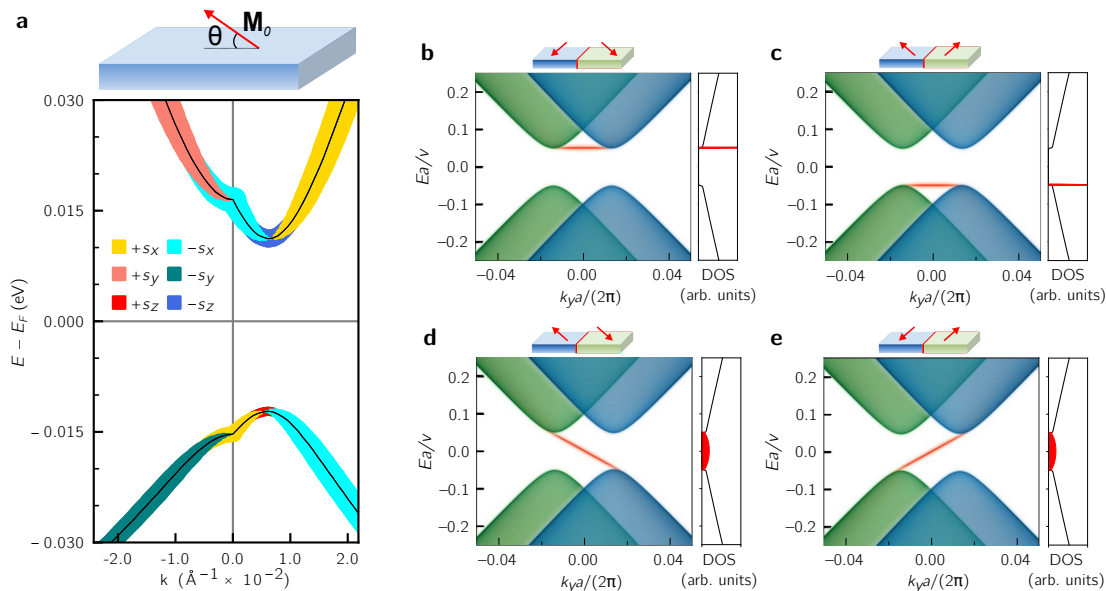


FIG. 3. (a) $\text{MnBi}_2\text{Te}_2\text{Se}_2$ surface band structure near the Fermi level in the case of mixed magnetization. (b, c, d, e) The same as Fig. 2b but with additional negative (b), positive (c) and opposite (d, e) out-of-plane magnetization components.

applying an external magnetic field perpendicular to the surface plane. In this context, AFM TIs with the in-plane sublattice magnetization provide a very special and rich platform to study surface electronic properties.

The appearance of flat bands with fully spin-polarized electron states leads to some unusual effects in these materials. For example, the optical excitation of electrons from the flat band can lead to an observable spin-resolved photoelectric effect, e.g. spin- and valley-polarized currents.

The flat band state can manifest itself in the anomalous Hall effect on a single DW. Indeed, free electrons in the uppermost SL, transmitted through the DW, are subjected to the out-of-plane polarisation associated with the state. Due to SOC it can lead to the transverse current.

Since the Fermi energy is pinned at the flat band energy, we can also predict the appearance of superconductivity related to the coupling of heavy electrons from the neighboring DWs. Indeed, the electrons from neighboring DWs have opposite spin directions, and the interaction between them via phonons can be rather strong since the electron localization allows to release the momentum conservation condition in the electron-phonon interaction. It should be also noted that the intra-DW electron-electron repulsion does not affect the superconductivity related to pairing at different DWs⁴⁵. Finally, we can expect an enhancement of the critical temperature for superconductivity transition thanks to an infinite electron density of states.

Appendix: Methods

Bulk crystal structures, magnetic order, MAE, bulk and surface band structures were investigated using the projector augmented-wave method (PAW)⁴⁶ implemented in VASP package⁴⁷⁻⁴⁹. Exchange-correlation effects were taken into account using Perdew-Burke-Ernzerhof generalized gradient approximation (GGA)⁵⁰. Spin-orbit coupling was treated using the second variation technique⁵¹. DFT-D3 method⁵² was used to accurately describe the van der Waals interaction. The plane wave energy cutoff was chosen exclusively for each compound (280 eV for $\text{MnBi}_2\text{Te}_2\text{Se}_2$, 240 eV for VBi_2Se_4 , $\text{VBi}_2\text{Te}_2\text{Se}_2$ and VBi_2Te_4 , 275 eV for $\text{VSb}_2\text{Te}_2\text{Se}_2$ and 250 eV for VSb_2Te_4) and was kept constant through all calculations. The energy convergence criterion was set to 10^{-6} eV for all types of calculations except magnetocrystalline anisotropy study, for which it was decreased down to 10^{-7} eV. FM phases were modeled using a rhombohedral cell containing one Mn or V atom (1 f.u.) and monoclinic cell containing 4 Mn or V atoms (4 f.u.), respectively. AFM bulk phases was modeled using rhombohedral cell, containing 2 Mn atoms (2 f.u.) and hexagonal cell, containing 6 Mn atoms (6 f.u.). Collinear AFM and non-collinear AFM phases were modeled using rectangular ($1 \times \sqrt{3}$) and ($\sqrt{3} \times \sqrt{3}$) $R30^\circ$ cell, respectively. All ferromagnetic slabs were studied using convenient hexagonal cell. Magnetocrystalline anisotropy studies were performed on the same hexagonal cell. Surfaces were modeled within repeating slabs model.

Mn and V $3d$ -states were treated using a GGA+ U approach^{53,54}. The values of U_{eff} were calculated using a linear response technique proposed by Cococcioni et al.⁵⁵ Adopted U values were 5.3, 4.8, 5.0, 4.7, 4.6 and

5.0 eV for $\text{MnBi}_2\text{Te}_2\text{Se}_2$, VBi_2Se_4 , $\text{VBi}_2\text{Te}_2\text{Se}_2$, VBi_2Te_4 , $\text{VSb}_2\text{Te}_2\text{Se}_2$ and VSb_2Te_4 respectively. Also we looked into other close U_{eff} values and we did not find any qualitative changes in calculation results.

Calculations of \mathbb{Z}_2 invariants were performed using Z2Pack⁵⁶⁻⁵⁹.

In order to obtain exchange coupling parameters, we used the magnetic force theorem⁶⁰ as it is implemented within the multiple scattering theory package Hutsepot⁶¹, along with the full charge density approximation⁶². They were confirmed by Monte-Carlo simulations based on the classical Heisenberg Hamiltonian with the obtained exchange coupling parameters from above. The heat capacity was used as indication for the magnetic phase transition. Monte Carlo results were checked for convergence of all simulation parameters, i.e., simulation size and Monte Carlo steps. More technical details can be found in Ref.⁶¹.

The introduced toy model, Eq. (1), may be directly implemented to analytically describe low-energy fermions at the surface of planar AFM TI for various inhomogeneous magnetization configurations in uppermost SL. This consideration is restricted to simple configurations (in the form of rigid one-dimensional DWs) which allowed us to find the exact solution for the corresponding eigenstate problem. Indeed, we have obtained a modification of the energy spectrum and the envelope wave function spatial profile of the surface states caused by a magnetic DW presence. These results are consistent with those of tight-binding study of the model regularized on square lattice.

ACKNOWLEDGMENTS

We are thankful for support from Tomsk State University competitiveness improvement programme (project

8.1.01.2018) and from Saint Petersburg State University (Grant ID 40990069). E.K.P. acknowledges support from RFBR within the research projects No. 18-32-00728 (the study of V-based compounds crystal, magnetic and band structures) and No. 19-32-90250 (the study of V-based compounds critical temperatures). V.N.M., T.V.M. and I.P.R. acknowledge support from RSF within the research project No. 18-12-00169 (the study DWs by model Hamiltonian and tight-binding approaches). A.E. acknowledges support from DFG through priority program SPP1666 (Topological Insulators) and OeAD Grants No. HR 07/2018 and No. PL 03/2018. V.K.D. acknowledges support from the National Science Center of Poland under the project No. DEC-2017/27/B/ST3/02881. E.V.C. acknowledges support from RFBR within the research project No. 18-52-06009. Calculations performed at the Research Park of St.-Petersburg State University ‘‘Computing Center’’ and SKIF-Cyberia supercomputer of National Research Tomsk State University.

AUTHOR CONTRIBUTIONS

First-principles calculations were performed by E.K.P. and A.E. Monte-Carlo simulations were done by M.H. Model Hamiltonian approach was developed by V.N.M. Tight-binding calculations were performed by I.P.R. Figures were produced by E.K.P., T.V.M. and I.P.R. Project planning was done by E.V.C., E.K.P., T.V.M., I.P.R., V.N.M. and A.E. All authors contributed to the discussion and to writing the manuscript.

* evg.konst.petrov@gmail.com

† evguenivladimirovich.tchoulkov@ehu.eus

¹ C. L. Kane and E. J. Mele, Physical review letters **95**, 226801 (2005).

² C. L. Kane and E. J. Mele, Physical review letters **95**, 146802 (2005).

³ H. Weng, R. Yu, X. Hu, X. Dai, and Z. Fang, Advances in Physics **64**, 227 (2015).

⁴ L. Ju, Z. Shi, N. Nair, Y. Lv, C. Jin, J. Velasco Jr, C. Ojeda-Aristizabal, H. A. Bechtel, M. C. Martin, A. Zettl, *et al.*, Nature **520**, 650 (2015).

⁵ T. Y. Hung, K. Y. Camsari, S. Zhang, P. Upadhyaya, and Z. Chen, Science advances **5**, eaau6478 (2019).

⁶ E. Mania, A. Cadore, T. Taniguchi, K. Watanabe, and L. Campos, Communications Physics **2**, 6 (2019).

⁷ M. Sui, G. Chen, L. Ma, W.-Y. Shan, D. Tian, K. Watanabe, T. Taniguchi, X. Jin, W. Yao, D. Xiao, *et al.*, Nature Physics **11**, 1027 (2015).

⁸ X.-T. He, E.-T. Liang, J.-J. Yuan, H.-Y. Qiu, X.-D. Chen, F.-L. Zhao, and J.-W. Dong, Nature communications **10**, 872 (2019).

⁹ B. Lian, Z. Wang, and B. A. Bernevig, Physical review letters **122**, 257002 (2019).

¹⁰ X. Lu, P. Stepanov, W. Yang, M. Xie, M. A. Aamir, I. Das, C. Urgell, K. Watanabe, T. Taniguchi, G. Zhang, *et al.*, arXiv preprint arXiv:1903.06513 (2019).

¹¹ H. C. Po, L. Zou, A. Vishwanath, and T. Senthil, Physical Review X **8**, 031089 (2018).

¹² M. Yankowitz, S. Chen, H. Polshyn, Y. Zhang, K. Watanabe, T. Taniguchi, D. Graf, A. F. Young, and C. R. Dean, Science **363**, 1059 (2019).

¹³ Y. Cao, V. Fatemi, S. Fang, K. Watanabe, T. Taniguchi, E. Kaxiras, and P. Jarillo-Herrero, Nature **556**, 43 (2018).

¹⁴ E. H. Lieb, Physical review letters **62**, 1201 (1989).

¹⁵ A. Mielke, Journal of Physics A: Mathematical and General **24**, 3311 (1991).

- ¹⁶ A. Tanaka and H. Ueda, *Physical review letters* **90**, 067204 (2003).
- ¹⁷ H. Katsura, I. Maruyama, A. Tanaka, and H. Tasaki, *EPL (Europhysics Letters)* **91**, 57007 (2010).
- ¹⁸ E. Tang and L. Fu, *Nature Physics* **10**, 964 (2014).
- ¹⁹ Y. Cao, V. Fatemi, A. Demir, S. Fang, S. L. Tomarken, J. Y. Luo, J. D. Sanchez-Yamagishi, K. Watanabe, T. Taniguchi, E. Kaxiras, *et al.*, *Nature* **556**, 80 (2018).
- ²⁰ N. Y. Fogel, E. Buchstab, Y. V. Bomze, O. Yuzepovich, M. Y. Mikhailov, A. Y. Sipatov, E. Pashitskii, R. Shekhter, and M. Jonson, *Physical Review B* **73**, 161306 (2006).
- ²¹ O. Mironov, B. Savitskii, A. Y. Sipatov, A. Fedorenko, A. Chirkin, S. Chistyakov, and L. Shpakovskaya, *JETP Lett* **48** (1988).
- ²² Y. Cao, V. Fatemi, S. Fang, K. Watanabe, T. Taniguchi, E. Kaxiras, and P. Jarillo-Herrero, *Nature* **556**, 43 EP (2018), article.
- ²³ C. Gong, L. Li, Z. Li, H. Ji, A. Stern, Y. Xia, T. Cao, W. Bao, C. Wang, Y. Wang, *et al.*, *Nature* **546**, 265 (2017).
- ²⁴ B. Huang, G. Clark, E. Navarro-Moratalla, D. R. Klein, R. Cheng, K. L. Seyler, D. Zhong, E. Schmidgall, M. A. McGuire, D. H. Cobden, *et al.*, *Nature* **546**, 270 (2017).
- ²⁵ M. Otrokov, T. Menshchikova, M. Vergniory, I. Rusinov, A. Y. Vyazovskaya, Y. M. Koroteev, G. Bihlmayer, A. Ernst, P. Echenique, A. Arnau, *et al.*, *2D Materials* **4**, 025082 (2017).
- ²⁶ M. M. Otrokov, T. V. Menshchikova, I. P. Rusinov, M. G. Vergniory, V. M. Kuznetsov, and E. V. Chulkov, *JETP Lett.* **105**, 297 (2017).
- ²⁷ T. Hirahara, S. V. Eremeev, T. Shirasawa, Y. Okuyama, T. Kubo, R. Nakanishi, R. Akiyama, A. Takayama, T. Hattori, S.-i. Ideta, *et al.*, *Nano letters* **17**, 3493 (2017).
- ²⁸ D. R. Klein, D. MacNeill, J. L. Lado, D. Soriano, E. Navarro-Moratalla, K. Watanabe, T. Taniguchi, S. Manni, P. Canfield, J. Fernández-Rossier, *et al.*, *Science* **360**, 1218 (2018).
- ²⁹ T. Song, X. Cai, M. W.-Y. Tu, X. Zhang, B. Huang, N. P. Wilson, K. L. Seyler, L. Zhu, T. Taniguchi, K. Watanabe, *et al.*, *Science* **360**, 1214 (2018).
- ³⁰ Z. Wang, I. Gutiérrez-Lezama, N. Ubrig, M. Kroner, M. Gibertini, T. Taniguchi, K. Watanabe, A. Imamoglu, E. Giannini, and A. F. Morpurgo, *Nature communications* **9**, 2516 (2018).
- ³¹ R. S. Mong, A. M. Essin, and J. E. Moore, *Physical Review B* **81**, 245209 (2010).
- ³² M. A. McGuire, H. Dixit, V. R. Cooper, and B. C. Sales, *Chemistry of Materials* **27**, 612 (2015).
- ³³ P. M. Sass, W. Ge, J. Yan, D. Obeysekera, J. Yang, and W. Wu, *arXiv preprint arXiv:1910.06488* (2019).
- ³⁴ K. Yasuda, M. Mogi, R. Yoshimi, A. Tsukazaki, K. Takahashi, M. Kawasaki, F. Kagawa, and Y. Tokura, *Science* **358**, 1311 (2017).
- ³⁵ I. T. Rosen, E. J. Fox, X. Kou, L. Pan, K. L. Wang, and D. Goldhaber-Gordon, *npj Quantum Materials* **2**, 69 (2017).
- ³⁶ S. V. Eremeev, G. Landolt, T. V. Menshchikova, B. Slomski, Y. M. Koroteev, Z. S. Aliev, M. B. Babanly, J. Henk, A. Ernst, L. Patthey, *et al.*, *Nature communications* **3**, 635 (2012).
- ³⁷ M. Otrokov, I. Klimovskikh, H. Bentmann, D. Estyunin, A. Zeugner, Z. Aliev, S. Gaß, A. Wolter, A. Koroleva, A. Shikin, *et al.*, *Nature* **576**, 416 (2019).
- ³⁸ M. M. Otrokov, I. P. Rusinov, M. Blanco-Rey, M. Hoffmann, A. Y. Vyazovskaya, S. V. Eremeev, A. Ernst, P. M. Echenique, A. Arnau, and E. V. Chulkov, *Phys. Rev. Lett.* **122**, 107202 (2019).
- ³⁹ I. Klimovskikh, M. Otrokov, D. Estyunin, S. Eremeev, S. Filnov, A. Koroleva, E. Shevchenko, V. Voroshnin, I. Rusinov, M. Blanco-Rey, *et al.*, *arXiv preprint arXiv:1910.11653* (2019).
- ⁴⁰ J. Wu, F. Liu, M. Sasase, K. Ienaga, Y. Obata, R. Yukawa, K. Horiba, H. Kumigashira, S. Okuma, T. Inoshita, *et al.*, *Science advances* **5**, eaax9989 (2019).
- ⁴¹ B. Chen, F. Fei, D. Zhang, B. Zhang, W. Liu, S. Zhang, P. Wang, B. Wei, Y. Zhang, Z. Zuo, *et al.*, *Nature communications* **10**, 1 (2019).
- ⁴² S. Eremeev, M. Otrokov, and E. Chulkov, *Journal of Alloys and Compounds* **709**, 172 (2017).
- ⁴³ J. R. Viana and J. R. de Sousa, *Physical Review B* **75**, 052403 (2007).
- ⁴⁴ N. D. Mermin and H. Wagner, *Physical Review Letters* **17**, 1133 (1966).
- ⁴⁵ K. Efetov and A. Larkin, *Zh. Eksp. Teor. Fiz* **68**, 155 (1975).
- ⁴⁶ P. E. Blöchl, *Physical review B* **50**, 17953 (1994).
- ⁴⁷ G. Kresse and J. Hafner, *Physical Review B* **47**, 558 (1993).
- ⁴⁸ G. Kresse and J. Furthmüller, *Physical review B* **54**, 11169 (1996).
- ⁴⁹ G. Kresse *et al.*, *Comput. Mater. Sci.* **6**, 15 (1996).
- ⁵⁰ J. P. Perdew, K. Burke, and M. Ernzerhof, *Physical review letters* **77**, 3865 (1996).
- ⁵¹ D. Koelling and B. Harmon, *Journal of Physics C: Solid State Physics* **10**, 3107 (1977).
- ⁵² S. Grimme, J. Antony, S. Ehrlich, and H. Krieg, *The Journal of chemical physics* **132**, 154104 (2010).
- ⁵³ V. I. Anisimov, J. Zaanen, and O. K. Andersen, *Physical Review B* **44**, 943 (1991).
- ⁵⁴ S. Dudarev, G. Botton, S. Savrasov, C. Humphreys, and A. Sutton, *Physical Review B* **57**, 1505 (1998).
- ⁵⁵ M. Cococcioni and S. De Gironcoli, *Physical Review B* **71**, 035105 (2005).
- ⁵⁶ A. A. Soluyanov and D. Vanderbilt, *Physical Review B* **83**, 235401 (2011).
- ⁵⁷ D. Gresch, G. Autes, O. V. Yazyev, M. Troyer, D. Vanderbilt, B. A. Bernevig, and A. A. Soluyanov, *Physical Review B* **95**, 075146 (2017).
- ⁵⁸ N. Marzari and D. Vanderbilt, *Physical review B* **56**, 12847 (1997).
- ⁵⁹ A. A. Mostofi, J. R. Yates, Y.-S. Lee, I. Souza, D. Vanderbilt, and N. Marzari, *Computer physics communications* **178**, 685 (2008).
- ⁶⁰ A. I. Liechtenstein, M. Katsnelson, V. Antropov, and V. Gubanov, *Journal of Magnetism and Magnetic Materials* **67**, 65 (1987).
- ⁶¹ M. Hoffmann, Arthur Ernst, W. Hergert, V. N. Antonov, W. A. Adeagbo, R. M. Geilhufe, and H. Ben Hamed, *physica status solidi (b)* (2020).
- ⁶² L. Vitos, J. Kollár, and H. L. Skriver, *Physical Review B* **49**, 16694 (1994).

Supplementary Information for: Domain wall induced spin-polarized flat bands in antiferromagnetic topological insulators

E. K. Petrov,^{1,2,*} V. N. Men'shov,^{3,1,2} I. P. Rusinov,^{1,2} M. Hoffmann,⁴ A. Ernst,^{4,5}
M. M. Otrokov,^{6,7} V. K. Dugaev,⁸ T. V. Menshchikova,¹ and E. V. Chulkov^{9,10,2,6,1}

¹Tomsk State University, 634050 Tomsk, Russia

²St. Petersburg State University, 199034 St. Petersburg, Russia

³NRC Kurchatov Institute, 123182 Moscow, Russia

⁴Institute for Theoretical Physics, Johannes Kepler University, 4040 Linz, Austria

⁵Max Planck Institute of Microstructure Physics, 06120 Halle, Germany

⁶Centro de Física de Materiales (CFM-MPC), Centro Mixto CSIC-UPV/EHU,
20018 Donostia-San Sebastián, Basque Country, Spain

⁷IKERBASQUE, Basque Foundation for Science, 48011 Bilbao, Spain

⁸Department of Physics and Medical Engineering,

Rzeszów University of Technology, 35-959 Rzeszów, Poland

⁹Departamento de Física de Materiales, Facultad de Ciencias Químicas,

Universidad del País Vasco, Apdo. 1072, 20080 San Sebastián/Donostia, Spain

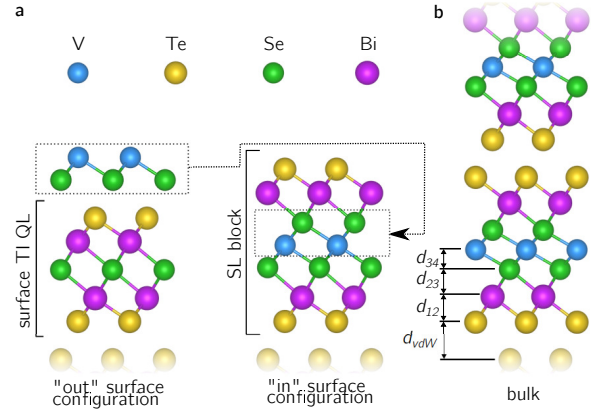
¹⁰Donostia International Physics Center (DIPC), 20018 San Sebastián/Donostia, Spain

(Dated: February 1, 2022)

SUPPLEMENTARY NOTE 1: EQUILLIBRIUM CRYSTAL STRUCTURE AND FORMATION ENERGIES

According to the last reports¹, MnSe bilayer tends to diffuse from Bi₂Se₃ surface to the center of topmost TI QL, forming an MnBi₂Se₄ SL. In order to show, that similar process is possible for monochalcogenides VSe, VTe and MnSe deposited on the surface of a typical TI (Bi₂Se₃, Bi₂Te₂Se, Bi₂Te₃, Sb₂Te₂Se or Sb₂Te₃) surface, we focus on total energy comparison of “out” (deposited bilayer is located on the TI QL surface) and “in” (deposited bilayer is located in TI QL center) configurations for VSe/Bi₂Se₃, VSe/Bi₂Te₂Se, VTe/Bi₂Te₃, VSe/Sb₂Te₂Se, VTe/Sb₂Te₃ and MnSe/Bi₂Te₂Se pairs without considering the diffusion mechanism of deposited atoms inside the QL (Suppl. Fig. 1). In “out” configuration the deposited bilayer can be oriented in two ways: forming V or Se (Te) termination, respectively. We found V termination to be preferable for VSe/Bi₂Se₃ and VSe/Bi₂Te₂Se cases, while VTe/Bi₂Te₃ prefers Te one. Comparison of the total energy of “out” and “in” configurations clearly indicates that VSe (VTe) diffusion to the topmost QL center is more favorable (Table 1).

Note, one of the necessary conditions for introducing a magnetic monochalcogenide bilayer to the center of topmost TI structural block is small in-plane lattice mismatch of the bilayer and substrate. It was shown that the V-based monochalcogenides can exhibit hexagonal NiAs-type (NA) and wurtzite-type (WZ) phases but the last one was not yet obtained experimentally. However, using ab-initio approach, their equilibrium lattice parameters were calculated². Similarly to the MnSe, resulting WZ phase lattice parameters of V-based monochalcogenides match with substrate much better than NA ones and guarantee the possibility of well structured SL formation.



Supplementary Figure 1. (a) VBi₂Te₂Se₂ SL formation scheme. (b) Bulk interplane distances notation.

Since a magnetic SL can be formed on a TI surface, thick magnetic films can be also constructed. For example, VSe deposition on Bi₂Se₃ surface will create one VBi₂Se₄ SL. After that, one Bi₂Se₃ QL may be deposited over VBi₂Se₄ SL, and this process may be repeated. By doing so, it is possible to grow a magnetic film thick enough to bulk electronic properties starting to emerge. Hence, bulk crystal and electronic structure investigation is vital for a complete analysis of compounds under study.

As it was mentioned in the main text, in the case of VBi₂Se₄ total energy difference between rhombohedral and monoclinic structure is about 100 times less than in all other considered cases. Since at this stage all compounds were assumed to be FM, such small energy profit may indicate that monoclinic magnetic ground state may be AFM. We considered 4 different types of AFM order (AFM-1, AFM-2, AFM-3, AFM-4, see Ref.³) of monoclinic VBi₂Se₄, and found its magnetic ground state to be FM. Considered AFM orders were found to exhibit

total energies higher than FM one by 0.307 meV/f.u., 5.09 meV/f.u., 5.09 meV/f.u. and 5.244 meV/f.u. for AFM-1, AFM-2, AFM-3, AFM-4 orders, respectively.

Supplementary Table 1. Total energy difference between “out” (E_{out}) and “in” (E_{in}) surface configurations. Positive value means that “in” configuration is favorable. First element in the first column indicated preferable termination in “out” configuration (e.g., TeV/Bi₂Te₃ prefers Te termination and VSe/Bi₂Te₂Se prefers Se termination as it shown on Suppl. Fig. 1a).

System	$E_{out} - E_{in}(eV/f.u.)$
MnSe/Bi ₂ Te ₂ Se	0.470
VSe/Bi ₂ Se ₃	1.063
VSe/Bi ₂ Te ₂ Se	0.983
TeV/Bi ₂ Te ₃	0.861
TeV/Sb ₂ Te ₃	0.95
SeV/Sb ₂ Te ₂ Se	1.021

Supplementary Table 2. Total energy difference between monoclinic (E_{min}) and rhombohedral (E_{rhomb}) bulk phases. The energy units are meV/f.u. Positive value means that rhombohedral bulk phase is favorable.

System	$E_{mon} - E_{rhomb}$ (meV/f.u.)
MnBi ₂ Te ₂ Se ₂	+225.5
VBi ₂ Se ₄	+0.9
VBi ₂ Te ₂ Se ₂	+318.3
VBi ₂ Te ₄	+180.6
VSb ₂ Te ₂ Se ₂	+239.8
VSb ₂ Te ₄	+116.8

Supplementary Table 3. Lattice parameters and inter-layer distances of rhombohedral bulk phases. All units are angstroms.

System	a_{hex}	d_{12}	d_{23}	d_{34}	d_{vdW}
MnBi ₂ Te ₂ Se ₂	4.1904	1.82863	1.95850	1.40135	2.70315
VBi ₂ Se ₄	4.0783	1.60575	1.99966	1.42537	2.49110
VBi ₂ Te ₂ Se ₂	4.1906	1.82349	1.94649	1.38162	2.75384
VBi ₂ Te ₄	4.3380	1.75433	2.11106	1.53298	2.59393
VSb ₂ Te ₂ Se ₂	4.1124	1.76196	1.86362	1.41252	2.88337
VSb ₂ Te ₄	4.2605	1.69003	2.02189	1.58758	2.69557

SUPPLEMENTARY NOTE 2: BAND STRUCTURES

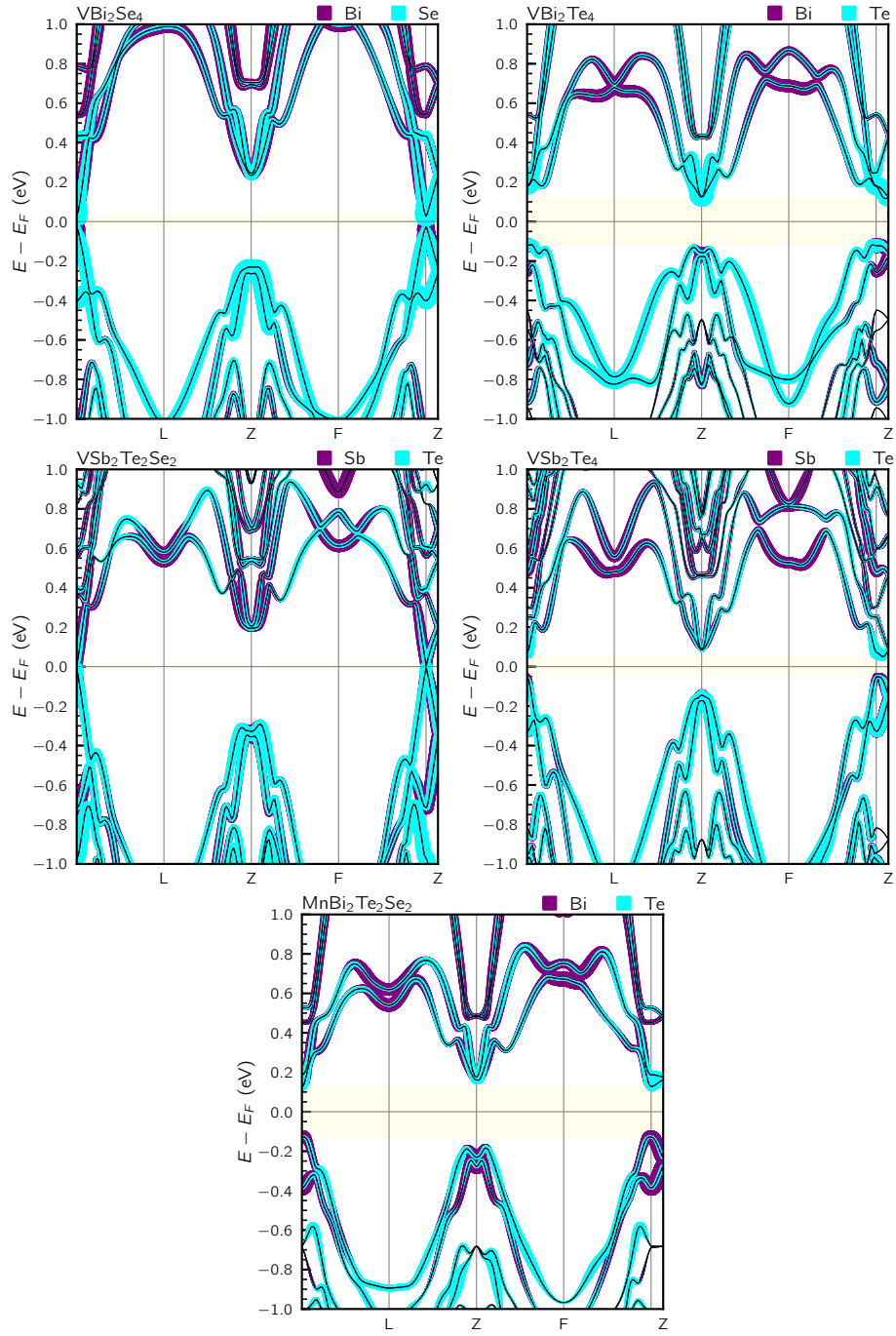
Here we present the band structures, which were not shown in the main text (see Suppl. Fig. 2 for bulk and Suppl. Fig. 3 for surface band structures, respectively). We do not show surface band structures of compounds which exhibit $\mathbb{Z}_2 = 0$ (see Table in the main text).

* evg.konst.petrov@gmail.com

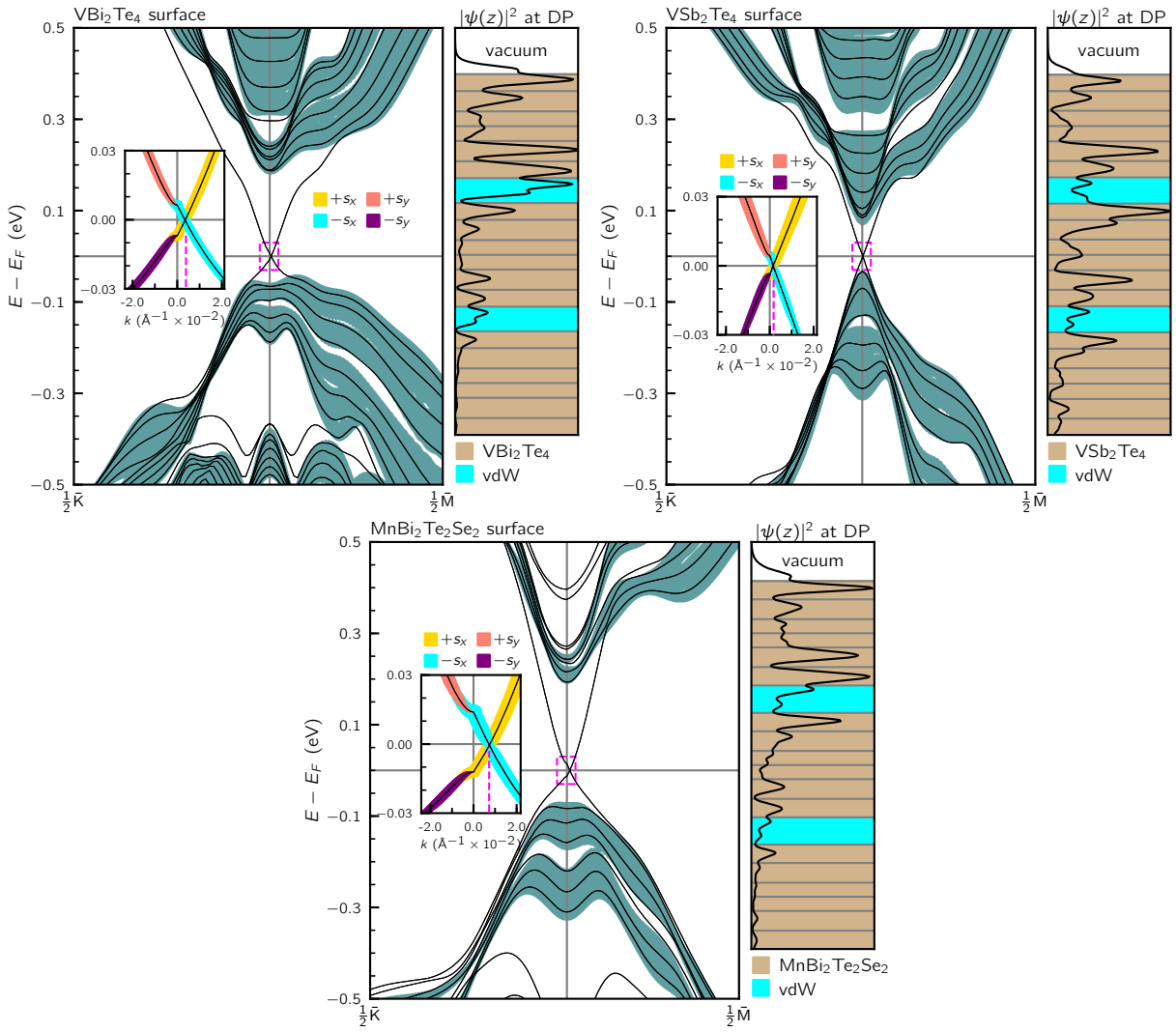
¹ T. Hirahara, S. V. Eremeev, T. Shirasawa, Y. Okuyama, T. Kubo, R. Nakanishi, R. Akiyama, A. Takayama, T. Hagiiri, S.-i. Ideta, *et al.*, Nano letters **17**, 3493 (2017).

² W.-H. Xie, B.-G. Liu, and D. Pettifor, Physical Review B **68**, 134407 (2003).

³ S. Eremeev, M. Otrokov, and E. Chulkov, Journal of Alloys and Compounds **709**, 172 (2017).



Supplementary Figure 2. VBi_2Se_4 , VBi_2Te_4 , $\text{VSb}_2\text{Te}_2\text{Se}_2$, VSb_2Te_4 and $\text{MnBi}_2\text{Te}_2\text{Se}_2$ bulk band structures near the Fermi level. Notations are the same as in Fig. 2c in the main text.



Supplementary Figure 3. VBi_2Te_4 , VSb_2Te_4 and $\text{MnBi}_2\text{Te}_2\text{Se}_2$ surface band structures. Notations are the same as in Fig. 3a in the main text.